

ENVIRONMENTAL IMPACT ASSESSMENT USING NEURAL NETWORK MODEL: A CASE STUDY OF THE JAHANI, KONARSAH AND KOHE GACH SALT PLUGS, SE SHIRAZ, IRAN

M. H. Tayebi^{a,*}, M. H. Tangestani^a, H. Roosta^b

^a Dept. of Earth sciences, Faculty of sciences, Shiraz University, 71454, Shiraz, Iran- Mhtayebi@shirazu.ac.ir- Tangestani@susc.ac.ir

^b Dept. of Civil Engineering, Marvdasht Branch, Islamic Azad University, Marvdasht, Iran – Hasan.Roosta@gmail.com

KEY WORDS: Salt plug, Environmental impact, MLP neural network, ASTER

ABSTRACT:

This study employs Multi-Layer Perceptron (MLP) to estimate environmental impact of salt plugs using Advanced Spaceborne Thermal Emission and Reflection Radiometer (ASTER). VNIR and SWIR datasets of ASTER were assessed in mapping and detecting Jahani, Konarsiah, and Kohe Gach salt plugs and the affected areas located at SE Shiraz, Iran. PC color composite and geological map of the region were used to select training areas. Three datasets including, IARR, PCA and MNF were used as input to the MLP. The results of each input were compared with the ground truth and the geological map to determine the accuracy and therefore to select the more appropriate dataset to be input to MLP approach input. The results demonstrated a number of the polluted sites and the main polluted tributaries that convey the water as well as the salt plug materials into the Firouzabad River. It is also indicated that the MNF input (with 85% overall accuracy) can obtain a slightly more accurate estimation than the IARR (79%) and PCA inputs (82%). It is concluded that the result of MNF input to MLP is more applicable to effective environmental impact assessment and sustainable water resources management at salt plug-affected areas.

1. INTRODUCTION

Salinity caused by natural processes is a major environmental hazard and can have hazardous effects on agricultural production, water quality, ecological health, soil erosion, flood risk, infrastructure and the society. The effects and damages of salinity are not stronger than earthquake or landslide (Metternicht and Zink, 2003), but it is a major threat in semi-arid and arid regions such as Iran. The most important impact of salinity is salinization of fresh rivers, which affects the quality of water for drinking and irrigation.

More than 150 known salt plugs (Kent, 1970) are exposed at the south eastern Zagros Folded Belt, southern Iran. These saline formations are important because: (1) they can potentially trap the hydrocarbons, (2) for their potential in ore deposition, and (3) they can provide harmful environmental impacts. Three of these salt plugs, namely Konarsiah, Jahani and Kohe Gach are exposed at the SE Shiraz, southern Firouzabad (Fig. 1). These salt plugs increase the salinity of groundwater, surface water (especially Firouzabad River), and the adjacent soils by direct dissolution and transport of soluble salt plug minerals, which directly influence the economy and ecosystem of the area.

Information on the extent of the salt plug-affected areas is required for effective environmental planning and sustainable water resources management. Assessing the spread of salinity by salt plugs has traditionally been implemented by geochemical, hydrologic, and geophysical (Zadneek, 2008; Ghanbarian, 2007; Dehghan, 2008) methods requiring the collection of numerous samples followed by laboratory measurements. However, remote sensing can act as an effective

means of detecting environmental pollution and is a useful tool for acquiring basic information particularly on a regional scale (Sabins, 1997). The task of identifying salinity largely depends on the peculiar way salts distribute at the soil surface and within the soil mantle, and on the capability of the remote sensing tools to identify salts (Zinck, 2001). Many remote sensing techniques and datasets have already been used to map salt-affected areas (Hunt and Salisbury, 1976; Hick and Russell, 1990; Mougnot *et al.*, 1993; Ben-Dor *et al.*, 2002; Metternicht and Zink, 2003; Farifteh *et al.*, 2006), but there is lack of a publication focusing on the application of remote sensing in mapping and detecting the salt plug environmental impact. An unpublished work of Tavakkoli (2008), however, used the ASTER data for enhancing the lithological units of the same salt plugs.

Artificial neural network (ANN) is an interconnected group of nodes using mathematical methods to process information. It is a self adaptive system, which can change its structure based on the internal or external information (Hu and Weng, 2009). Among all the techniques, artificial neural networks (ANN) have been widely used (Ji, 2000; Zhai *et al.*, 2006) due to its advantages over statistical methods (Bischof *et al.*, 1992) such as no assumption about the probabilistic models of data, robust in noisy environments, and the ability to learn complex patterns (Ji, 2000). Neural networks have been applied in the large number and wide variety of applications (Liu *et al.*, 2001; Kavzoglu & Mather, 2003; Verbeke *et al.*, 2004; Chormanski *et al.*, 2008; Hu and Weng, 2009). The primary aim of this study was identifying and mapping the salt plugs as well as the salt plug-affected areas. The second aim is to evaluating the use of

* Corresponding author. Dept. of Earth Sciences, Faculty of Sciences, Shiraz University, 71454 Shiraz, Iran. Tel: +9809177173319 ; fax: +982284572. Mhtayebi@shirazu.ac.ir.

different input datasets (IARR, PCA and MNF) in identifying the environmental impact of the salt plugs. Bands 1-9 of ASTER in combination with Principal Component Analysis (PCA), Minimum Noise Fraction (MNF) transformation and Multi-Layer Perceptron (MLP) were used in this study.

2. STUDY AREA

The study area ($28^{\circ} 31' - 28^{\circ} 53' N$; $52^{\circ} 16' - 52^{\circ} 33' E$) is situated in the Zagros fold-and-thrust belt, western the Iranian province of Fars, southeastern Shiraz, and about 25Km south west of Firouzabad (Fig. 1). The Zagros mountain range is divided into three tectonic zones from the NE to the SW: the High Zagros, the Zagros Simply Folded Belt, and the Zagros Foredeep Zone (Stöcklin 1968; Falcon, 1974). The study area is located in the Simply Folded Belt (SFB) which has particularly been studied owing to the salt plugs and its structure. The geology consists of Infracambrian diapirs (salt plugs) surrounded by the Cretaceous to recent formations.

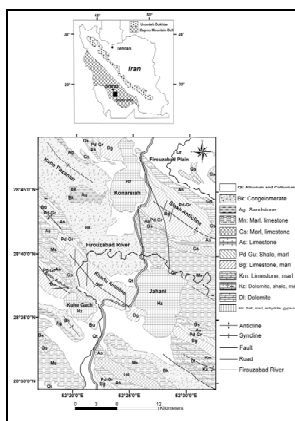


Figure 1. Geological map of the study area, Southern Firouzabad, SE Shiraz, Iran

3. METHODS

VNIR+SWIR dataset of ASTER were used to detect and map salt plugs-affected areas by the MLP neural network. ASTER instrument measures reflected radiation in three bands between 0.52 and 0.86 μm (VNIR) and six bands from 1.6 to 2.43 μm (SWIR), with 15- and 30-m resolution, respectively (Fujisada, 1995). The ASTER Level 1B data used in this study were acquired on March 24, 2001. The following steps constitute the data processing and analysis of the ASTER bands: (1) spatial registration of the 30-m SWIR data to the 15-m VNIR data; (2) the data were geometrically corrected using 1:25000 topographic maps; (3) Internal Average Relative Reflectance (IARR) calibration was then carried out on the data to normalizing images to a scene average spectrum. This method is particularly effective in areas where no ground measurements exist and little is known about the scene (Kruse, 1988); (4) A spectral reduction and data compression was performed using the principal components analysis; (5) To train and validate the use of MLP networks, training areas of each lithological unit were selected using knowledge of the PCA and the geological map. To do this, several ROIs were measured and extracted from ASTER image.

3.1 Principal Components Analysis (PCA)

Principal components analysis (Richards, 1984; Eklundh and Singh, 1993) has become a standard statistical approach in image processing for two main reasons: (1) to reduce the number of correlated image bands to form a small number of independent principal components to represent most of the variability carried by the multiple image bands, and (2) to increase the interpretability of the components as combinations of multiple bands (Jing and Panahi, 2006). PCA output results were used to create RGB color composite images to discriminating various lithological units and reducing the information included in the raw data into two or three bands without losing significant information (Monger, 2002).

Component	Eigenvalue	Variance (%)	Total (%)
PC1	0.2735	87.989	87.99
PC2	0.0238	7.661	95.65
PC3	0.0094	3.044	98.70
PC4	0.0016	0.520	99.22
PC5	0.0012	0.388	99.60
PC6	0.0005	0.173	99.78
PC7	0.0003	0.108	99.89
PC8	0.0001	0.060	99.95
PC9	0.0001	0.052	100.00

Table 1. PCA statistics of VNIR-SWIR ASTER bands on study area

PCA statistics were accounted to selecting components with the highest information to be used in selecting training areas. Table1 shows the eigenvalues, variances and total cumulative variances for the nine PC image of ASTER data. The PC1 image shows 87.99 percent of variances. The PC2 and PC3 images show 7.66 and 3.04 percent of variance respectively. Therefore the first three components represent 98.7% variances of the image data. On the other hand components 4-9 only contain 1.3% of the information.

In order to mapping lithology and environmental impact assessment of the salt plugs components 1-3 were used to generate colour composite image and to select training areas.

3.2 Minimum Noise Fraction (MNF)

The MNF transformation is a linear transformation related to principal components that orders the data according to signal-to-noise-ratio (Green *et al.*, 1988). It can be used to determine the inherent dimensionality of the data, to segregate noise in the data, and to reduce the computational requirements for subsequent processing (Green *et al.*, 1988; Boardman and Kruse, 1994). The MNF was applied to the ASTER to enhance lithological units and salt plugs-affected areas.

3.3 Multi-layer perceptron (MLP)

The multilayer perceptron (Rumelhart, and MacClelland, 1986) is by far the most well known and most popular neural network among all the existing neural network paradigms. (Hu and Neng Hwang, 2002; Carvalho, 2001). It is a mathematical approach (Hu and Weng, 2009), with some advantages and disadvantages as compared with other existing neural networks. For example, nonparametric statistical methods may be more useful for

describing the relationship between remotely sensed imagery and environmental variables since these tests make no a priori assumptions about the data. An artificial neural network (ANN) offers a powerful method for analyzing complex relationships among variables without making assumptions about the data. ANNs are capable of handling non-normality, nonlinearity and collinearity in a system (Haykin, 1994). There are many examples of successful MLP applications (Heermann, and Khazenie, 1992; Kanellopoulos, and Wilkinson, 1997; Verbeke, *et al.*, 2004; Roosta *et al.*, 2007; Hu and Weng, 2009). However, it is widely recognized that MLPs are sensitive to many operational factors including the size and quality of the training dataset, network architecture, training parameters, and over-fitting problems. (Yuan *et al.*, 2009; Kavzoglu and Mather, 2003). The parameters have to be set up properly to find the global minimum of error function instead of a local minimum (Hu and Weng, 2009).

A MLP neural network model used in the back-propagation (BP) learning algorithm has a nonlinear activation function (sigmoid function) contains several neurons (nodes), each having several inputs. These neurons are organized in layers, labeled as the hidden layer 1, hidden layer 2, and the output layer. Specifically to image classification, the input layer represents the original image, and each input layer node represents one image band. The hidden layer is used for image classification and passing the results to the output layer. The output layer outputs classified images (Hu and Weng, 2009). The name hidden layer refers to the fact that the output of these neurons will be fed into upper layer neurons and, therefore, is hidden from the user who only observes the output of neurons at the output layer (Yu and Neng Hwang, 2002). Figure 2 illustrates a configuration of MLP.

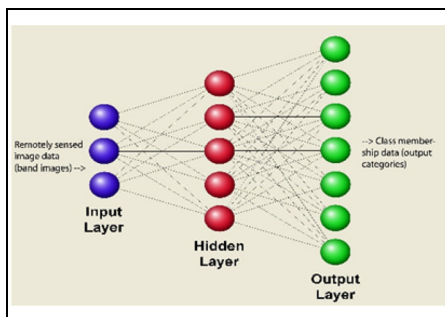


Figure 2. The structure of three-layer MLP neural network

The MLP approach consists of the following steps: (1) entering ASTER dataset as input (9 bands); (2) entering the training sites; (3) entering the number of training and testing sample pixels per category (The training pixels will be used in the analysis and will be a subset of the total pixels found in the training site). The testing pixels will be used to validate the results. The number of training samples will affect the accuracy of the training result. Too few samples may not represent the population for each category, while too many samples may cause samples to overlap, leading to a possible over training of the network. Additionally, too much iteration can also cause over training; (4) specifying the network topology (the number of hidden layers, the number of the input layer nodes, the number of the output layer nodes). The number of the hidden layer nodes is estimated by the following equation:

$$N_h = INT(\sqrt{N_i + N_o}) \quad (1)$$

Where N_h , N_i and N_o are the number of the hidden, input and output layer nodes respectively; (5) specifying the number of training parameters (the learning rate- the momentum factor- the stopping criteria- the number of iterations- set an accuracy rate); (6) training the network which is required to be implemented before classifying the image. Training a neural network is a key step in classification processes, the forward and backward passes continue until the network has "learned" the characteristics of all the classes and the neural network modified its internal representation by changing the values of its weights to improve the mapping of input to output relationships (Ziaai *et al.*, 2009). During training, each sample (for example, a feature vector associated with a single pixel) is fed into the input layer and the receiving node sums the weighted signals from all nodes to which it is connected in the preceding layer. Formally, the input that a single node receives is weighted according to:

$$net_j = \sum_{i=1}^m w_{ij} o_i \quad (2)$$

Where w_{ij} represents the weight between node i and j , and o_i is output from node i . The output from given node j is then computed from:

$$o_j = f(net_j) \quad (3)$$

The function f is usually a non-linear sigmoidal function that is applied to the weighted sum of inputs before the signal passes to the next layer.

Once the forward pass is finished, the activities of the output nodes are compared with their expected activities. Each node in the output layer is associated with a class. When a pattern is presented to the network, each output node will generate a value that indicates the similarity between the input pattern and the corresponding class. Except in very unusual circumstances, the actual output will differ from the desired outcome; the difference is associated with error in the network. This error is then propagated backward with weights for relevant connections corrected via a relation known as the delta rule:

$$\Delta w_{ij(t+1)} = \eta \delta_j o_i + \alpha \Delta w_{ij(t)} \quad (4)$$

Where η is the learning rate, α is the momentum factor, and δ_j is the computed error. The forward and backward passes continue until the network has "learned" the characteristics of all the classes. The purpose of training the network is to get the proper weights both for the connection between the input and hidden layer, and between the hidden and the output layer for the classification of the unknown pixels. The input pattern is classified into the class that is associated with the node with the highest activation level; (7) classifying image (hard classification image), and (8) accuracy assessment.

IARR, PCA and MNF datasets of ASTER were used as a first layer (the input layer) that is composed of nine neurons. Based on PC1, PC2 and PC3 color composite and exiting geological map, 7 training sites including salt plug (salt, gypsum, anhydrite), Bg (limestone, marl), Pd-Gu (shale, marl), As (limestone), Mn (marl, limestone), Bk (conglomerate) and Farmland were selected for defining the categories that should be classified. 100 pixels were used as training pixels and 100 pixels as testing pixels for validating the results. By using equation (1), 8 neurons were calculated to use in the hidden

layer and the 7 output layer nodes were defined based on the number of training site categories. For balance between training time and overall error reduction, learning rates between 0.01 - 0.2 were used, and to reduce the oscillatory problems, momentum factor between 0.5 and 0.6 were applied. To terminate the training process, the accuracy rate was set to 90% and 10000 iteration were chosen.

The more appropriate network parameters considered in this study were shown in table 2. For comparing the MLP results of IARR, PCA and MNF inputs this structure was used separately for each input. Three Hard classification images based on different input were produced by MLP approach to showing the lithological units and distribution of salt plug-affected areas (Fig 3).

Parameter	Value
Hidden layers	8
Learning rate	0.10
Momentum factor	0.5
Sigmoid constant a	1.0
Accurate rate %	90%

Table 2. The more appropriate network parameters that were used in this study.

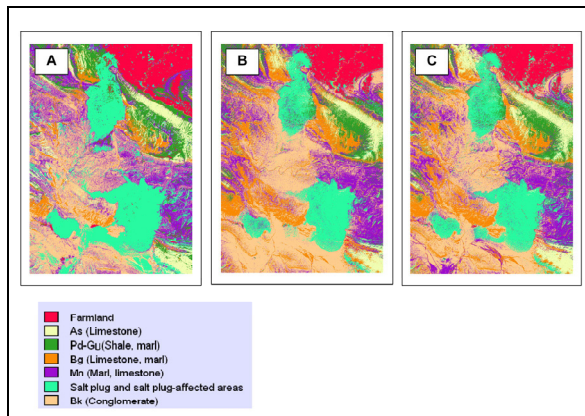


Figure 3. MLP mapping results, (A) result of IARR input to MLP, (B) result of PCA input to MLP, (C) result of MNF input to MLP.

4. ACCURACY ASSESSMENT OF INPUT DATASETS

To evaluate the results of MLP classification maps obtain from three input datasets (IARR, PCA and MNF), the accuracy of salt-affected areas and lithological units were assessed using ground reference information by determining the overall accuracy and Kappa coefficient.

The accuracy results are summarized in table 3. Comparison of the results of different input datasets shows higher capability of the MNF input to detect salt-affected areas. The accuracy results indicated that operating MLP with MNF input has higher accuracy (85%) than the IARR input with 79% accuracy and PCA inputs with 82% accuracy, so the hard classification image produced by MNF input was used to assessment of the salt plug-affected areas.

Input to MLP	Overall accuracy	Kappa coefficient
IARR	79%	0.64
PCA	82%	0.77
MNF	85%	0.79

Table 3. Accuracy assessment of hard classification maps

5. RESULT AND DISCUSSION

This study investigated the utility of the MLP network with different input (IARR, PCA and MNF) for detecting salt plug-affected areas southeastern Shiraz, Iran.

The ability to map salt plugs, and extent of the salt plug's materials are essential to understand and minimize salt plug's environmental impact and provides practical solutions to more advantageous water resources management.

At first, ASTER datasets of the area were analyzed by using the PCA method. By this method, the ASTER data were limited to 3 bands. Table 1 shows PCA eigen analysis of ASTER image. These components were used to find suitable training areas for the classification, as well as gathering sufficient number of training samples for each lithological unit with the aim of existing geological map. The training areas were used to training the MLP neural network and detecting salt plug-affected areas. Hard classification image of MNF input to MLP provide the opportunity to map salt plugs and salt plug-affected areas, as well as to estimate extent of salt plug materials. This may be important to identify impacts of salt plug on the adjacent areas, especially on the Firouzabad River (Fig 4).

The Jahani (central part of the scene), Konarsiah (upper part of the scene) and Kohe Gach (western part of the scene) were identified from this neural network method. The Hard classification image of the southern Firouzabad show Konarsiah salt plug in elliptical shape. This salt plug is located at the top of the image, surrounded by salt plug-affected areas along the slopes and margins of the salt plug (Fig 4). Yellow boxes in figure 4 indicate polluted areas surrounding the Konarsiah. The spatial distribution of salt plug-affected areas observed in the hard classification image revealed three main spatial trends. Relatively, high distribution of salt plug materials is seen in the northern, southern and western parts of the Konarsiah. It seems that morphology of the salt plug plays a major role on the shaping of the salt plug-affected areas, because it controls the flow of surface runoff and hence the distribution of salt plugs materials. The main tributaries that convey water as well as Konarsiah salt plug materials are shown in figure 4, drainages 1, 2 and 3, including branches that convey the Konarsiah materials into the Firouzabad River. The branch 1, located at the northern Konarsiah salt plug, drains its materials toward the east, but branches 2 and 3 are situated in the eastern and western sides of this salt plug respectively, draining their materials toward the south.

The Jahani salt plug is located at the center of the hard classification image (Fig 4). High distributions of salt plug materials occur in the eastern, western and south western parts of the Jahani. This image shows that the salt plug materials are extending down to the Firouzabad River. The amounts of materials decrease from the salt plug to the Firouzabad River. The results show a good differentiation between salt plugs materials and other lithological units however, some misclassifications occur in south east Jahani salt plug due to the spectral similarities. The main tributaries that convey the water as well as the Jahani salt plug materials are shown in figure 4.

Drainages 4, 5, and 6, located at the western side, drain the salt materials toward the west.

The distribution patterns of salt plug materials show a similarity to the spatial pattern of the Firouzabad river tributaries (Fig 4). The most important part of Firouzabad River that was polluted directly by the salt plug is situated at the northern part of the Jahani. This contact was clearly detected by the image processing (Fig 4).

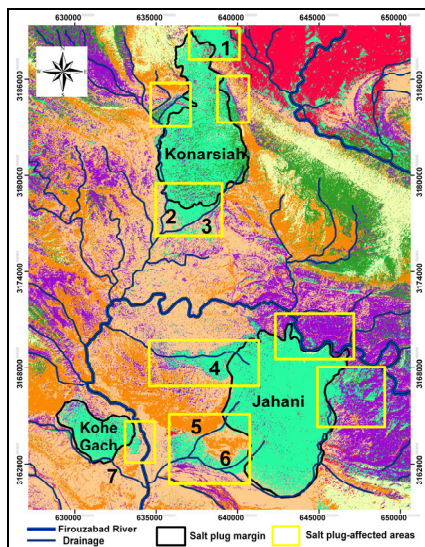


Figure 4. MLP mapping result, GIS layer of Firouzabad River and its tributaries are overlaid the image. Yellow boxes indicate the locations of polluted areas surrounding the Konarsiah, Jahani and kohe Gach. The labels 1, 2, 3, 4, 5, 6, and 7 illustrate the main polluted drainages.

Kohe Gach is a small salt plug and is located at the western part of the scene. The materials of this salt plug are identified as having the same composition as the Konarsiah and Jahani (Fig 4). Relatively high distribution of salt plug materials is seen in the eastern part of the Kohe Gach. This salt plug is another potential source of pollution, although the affected areas are relatively low. The main tributary that is polluted by this salt plug is branch number 7 (southern the salt plug), draining salt materials toward the east (Fig 4).

6. CONCLUSION

Results of MLP neural network at the south Firouzabad plain, SE Shiraz, demonstrated a number of the polluted sites and the main polluted tributaries that convey water as well as salt plug materials into the Firouzabad River. It is evident from the results that as water flows over and through the salt plugs, it picks up and carries contaminants towards the outlet of the basin. Surface water also carries pollutants into the underground water. Soil and the Firouzabad River, nearby the salt plugs, are polluted due to the erosion of these salt plugs. Therefore, it is necessary to plan to reduce their impacts on the water quality. Four affected areas around the Konarsiah salt plug, four affected areas surrounding the Jahani and one affected area adjacent to the Kohe Gach were identified and mapped using MLP approach.

Comparison of using different input to MLP approach showed that MNF input provides more accurate result than the IARR and PCA inputs. Results also demonstrated the viability of VNIR+SWIR dataset of ASTER in combination to the MLP approach for mapping the salt plugs and identifying their environmental impacts.

7. ACKNOWLEDGEMENT

The authors would like to thank the Research Vice Chancellor of Shiraz University, Iran. The ASTER data were provided by the Land Processes Distributed Active Center (LP DAAC), located at the U.S. Geological Survey (USGS) Earth Resources Observation and Science (EROS) Center.

8. REFERENCE

- Ben-Dor, E., 2002. Quantitative remote sensing of soil properties. *Advanced in Agronomy*, 75, pp. 173-243.
- Bischof, H.; Schneider, W.; Pinz, A.J., 1992. Multispectral classification of landsat images using neural networks. *IEEE Trans. Geosci. Remote Sens.* 30, pp. 482-490.
- Boardman J. W., and Kruse, F. A., 1994, Automated spectral analysis: A geologic example using AVIRIS data, north Grapevine Mountains, Nevada: in Proceedings, *Tenth Thematic Conference on Geologic Remote Sensing*, Environmental Research Institute of Michigan, Ann Arbor, MI, pp. I-407 - I-418.
- Carvalho, L. M. T., 2001. Mapping and monitoring forest remnants: A multiscale analysis of spatio-temporal data. Doctoral thesis. Wageningen University, Wageningen, The Netherlands.
- Chormanski, J., Voorde, T. V. D., Roeck, T. D., Batelaan, O., & Canters, F., 2008. Improving distributed runoff prediction in urbanized catchments with remote sensing based estimates of impervious surface cover. *Sensors*, 8, pp. 910-932.
- Dehghan Ghasr Ahmadi, M., 2008. Geological investigation of Sarvestan Salt dome and its influence on the Groundwater; MSc thesis, Dept. Of Earth Sciences, Shiraz University, Iran, pp. 119.
- Eklundh, L. and Singh, A., 1993. A comparative analysis of standardized and unstandardized principal components analysis in remote sensing. *International Journal of Remote Sensing*, 14, pp. 1359-1370.
- Falcon, N.L., 1974. Southern Iran: Zagros Mountains, in Mesozoic-Cenozoic Orogenic Belts, Data for Orogenic Studies, ed. Spencer, A.M., *Geol. Soc. Spec. Publ. London*, 4, pp. 199-211.
- Farifteh, j., Farshad, A. and George, R.J., 2006. Assessing salt-affected soils using remote sensing, solute modelling and geophysics, *Geoderma*, 130, pp. 191-206.
- Fujisada, H., 1995. Design and performance of ASTER instrument. *Proceedings SPIE* (International Society for Optical Engineering), Fujisada, H., Sweeting, M. N., eds, pp. 2583, 16-25.

- Ghanbarian, M. A., 2007. Tectonic and Geoelectrical studies of Salt domes in Southern fars with emphasis on Groundwater quality; MSc thesis, Dept. Of Earth Sciences, Shiraz University, Iran, pp. 230.
- Green, A. A., Berman, M., Switzer, B., and Craig, M. D., 1988. A transformation for ordering multispectral data in terms of image quality with implications for noise removal: *IEEE Transactions on Geoscience and Remote Sensing*, v. 26, no. 1, pp. 65 - 74.
- Haykin, S., 1994. Neural networks: A comprehensive foundation. Upper Saddle River, NJ7 Prentice Hall.
- Heermann, P.D., and Khazenie, N., 1992. Classification of multispectral remote sensing data using a backpropagation neural network. *IEEE Trans. Geosci. Remote Sens.*, 30, pp. 81–88.
- Hick, P.T., Russell, W.G.R., 1990. Some spectral considerations for remote sensing of soil salinity. *Aus. J. Soil Res.*, 28, pp. 417-431.
- Hunt, G., Salisbury J.W., 1976. Visible and near infrared spectra of minerals and rocks: XII. Metamorphic rocks. *Modern Geology*, 5, pp. 219-228.
- Hen Hu, Y and Neng Hwang, J., 2002. Hand book of neural network signal processing. CRC Press, pp. 1-1-1-30.
- Hu, X., and Weng, Q., 2009. Estimating impervious surfaces from medium spatial resolution imagery using the self-organizing map and multi-layer perceptron neural networks. *Remote Sensing of Environment*, 113, pp. 2089–2102.
- Ji, C. Y. (2000). Land-use classification of remotely sensed data using Kohonen selforganizing feature map neural networks. *Photogrammetric Engineering & Remote Sensing*, 66, pp. 1451–1460.
- Kanellopoulos, I., and Wilkinson, G.G. 1997. Strategies and best practice for neural network image classification. *Int. J. Remote Sens.*, 18, pp. 711–725.
- Kavzoglu, T., and Mather, P. M. 2003. The uses of backpropagating artificial neural networks in land cover classification. *International Journal of Remote Sensing*, 24(23), pp. 4907–4938.
- Kent, P.E., 1979. The emergent Hormuz salt diapirs of southern Iran, *J. Petrol. Geol.*, 2, pp. 117-144.
- Kruse, F.A., 1988. Use of airborne imaging spectrometer data to map minerals associated with hydrothermally altered rocks in the Northern Grapevine Mountains, Nevada, and California. *Remote Sens. Environ.* 24, pp. 31–51.
- Liu, J., Goering, C.E., Tian, L., 2001. A neural network for setting target corn yields. *Trans. ASAE* 44 (3), pp. 705–713.
- Metternicht, G.I., Zink, J.A., 2003. Remote sensing of soil salinity: potential and constraints. *Remote sensing of Environment*, 85, pp. 1-20.
- Monger, M., 2002. Soil classification in arid lands with Thematic Mapper data. *Terra*, 20(2), pp. 89-100.
- Mougenot, B., Pouget, M., Epema, G.F., 1993. Remote sensing of salt-affected soils. *Remote Sensing reviews*, 7, pp. 241-259.
- Jing, Q. C. L and Panahi, A., 2006. Principal component analysis with optimum order sample correlation coefficient for image enhancement. *International Journal of Remote Sensing*, 27(16), pp. 3387 - 3401.
- Richards, J.A., 1984. Thematic mapping from multitemporal image data using principal components transformation. *Remote Sensing of Environment*, 16, pp. 35-46.
- Roosta, H., Farhudi, R., Afifi M., 2007. Comparison between Sub-pixel Classifications of MODIS images: Linear Mixture Model and Neural Network Model, *WSEAS Transactions on Environment and Development*,
- Rumelhart, D.E, and MacClelland, J.L., 1986. Parallel Distributed Processing. *Explorations in the Microstructure of Cognition*, vol. I, MIT Press, Cambridge, MA.
- Sabins, F.F., 1997. Remote Sensing, Principles and Interpretation, third ed, Freeman, New York, pp. 494.
- Stöcklin, J., 1974. Possible ancient continental margin in Iran, In: Burk, C.A., Drake, C.L. (Eds.), *The Geology of Continental Margins*. Springer, Berlin, pp. 873–887.
- Tavakkoli, H., 2008. Comparison of TM and ASTER datasets for enhancement of lithological units of salt domes, a case study from Firouzabad area; MSc thesis, Dept. Of Earth Sciences, Shiraz University, Iran, pp.152.
- Verbeke, L.P.C., Vancoillie, F.M.B., De Wulf, R.R., 2004. Reusing back-propagation artificial neural networks for land cover classification in tropical savannahs. *Int. J. Remote Sens.*, 25, pp. 2747–2771.
- Yuan, H., Van Der Wiele, C. F., Khorram, S., 2009. An Automated Artificial Neural Network System for Land Use/Land Cover Classification from Landsat TM Imagery. *Remote Sens. I*, pp. 243-265.
- Zadneck, T., 2008. Environmental effects of Konarsiah Salt dome on pollution of water resource of Firouzabad area; MSc thesis, Dept. Of Earth Sciences, Shiraz University, Iran, pp.120.
- Zhai, Y., Thomasson, J.A., Boggess III, J.E., Sui, R., 2006. Soil texture classification with artificial neural networks operating on remote sensing data. *Computers and Electronics in Agriculture* 54 (2), pp. 53–68.
- Ziaii, M., a., Pouyan, A.A., Ziaei, M., 2009. Neuro-fuzzy modelling in mining geochemistry: Identification of geochemical anomalies. *Journal of Geochemical Exploration*. 100, pp. 25-36.
- Zinck, J. A., 2001. Monitoring salinity from remote sensing data. In R. Goossens, & B. M. De Vlieghe (Eds.), Proceedings of the 1st Workshop of the EARSeL Special Interest Group on Remote Sensing for Developing Countries (Belgium: Ghent University), pp. 359-368.